Enhanced energy storage behaviors in free-standing antiferroelectric $Pb(Zr_{0.95}Ti_{0.05})O_3$ thin membranes*

Zheng-Hu Zuo(左正笏)[1,2], Qing-Feng Zhan(詹清峰)[1,2,†], Bin Chen(陈斌)[1,2], Hua-Li Yang(杨华礼)[1,2], Yi-Wei Liu(刘宜伟)[1,2], Lu-Ping Liu(刘鲁萍)[1,2], Ya-Li Xie(谢亚丽)[1,2], and Run-Wei Li(李润伟)[1,2,‡]

[1] *Key Laboratory of Magnetic Materials and Devices, Ningbo Institute of Material Technology and Engineering, Chinese Academy of Sciences, Ningbo* 315201, *China*

[2] *Zhejiang Province Key Laboratory of Magnetic Materials and Application Technology, Ningbo Institute of Material Technology and Engineering, Chinese Academy of Sciences, Ningbo* 315201, *China*

(Received 23 February 2016; revised manuscript received 11 April 2016; published online 25 June 2016)

Free-standing antiferroelectric $Pb(Zr_{0.95}Ti_{0.05})O_3$ (PZT(95/5)) thin film is fabricated on 200-nm-thick Pt foil by using pulsed laser deposition. X-ray diffraction patterns indicate that free-standing PZT(95/5) film possesses an *a*-axis preferred orientation. The critical electric field for the 300-nm-thick free-standing PZT(95/5) film transiting from antiferroelectric to ferroelectric phases is increased to 770 kV/cm, but its saturation polarization remains almost unchanged as compared with that of the substrate-clamped PZT(95/5) film. The energy storage density and energy efficiency of the substrate-clamped PZT(95/5) film are 6.49 J/cm^3 and 54.5%, respectively. In contrast, after removing the substrate, the energy storage density and energy efficiency of the free-standing PZT(95/5) film are enhanced up to 17.45 J/cm^3 and 67.9%, respectively.

Keywords: antiferroelectric films, freestanding, energy storage

PACS: 77.80.–e, 68.55.–a, 84.60.Ve **DOI:** 10.1088/1674-1056/25/8/087702

1. Introduction

With the development of electronic devices towards miniaturization and light weight, electrical capacitors with high recoverable energy storage density and utilization are eagerly desired.[1–3] Currently, commercial high-power capacitors with energy density about 2.0 J/cm^3 are mostly made of linear dielectric polymer materials with low dielectric constant, e.g., polypropylene, polyethylene terephthalate, and polyphenylene sulfide, because of their high dielectric breakdown strengths.[2] Recently, antiferroelectric materials, in which dipole moments are alternatively aligned in the opposite directions, resulting in the zero net polarization, have become the promising candidates for application in high energy storage due to an electric field forced phase transition from antiferroelectric into the ferroelectric states. Compared with the commercial capacitor, the electrical capacitor made of antiferroelectric material may achieve a higher energy density (more than 10.0 J/cm^3)[4,5] and fast discharge speed (less than 20 ns).[6] Among various antiferroelectric materials, $PbZrO_3$ based antiferroelectric materials have received extensive attention, owing to their possible energy storage densities as high as 50 J/cm^3.[7] A lot of effort has been made to realize the theoretical prediction of energy storage density in the $PbZrO_3$ related antiferroelectric material by doping elements,[8,9] local field engineering[10] or changing electrode material.[11,12] For example, Parui and Krupanidhi obtained a remarkable energy storage density of 14.9 J/cm^3 at 600 kV/cm in La-doped $PbZrO_3$ thin film.[8] Sa *et al.*, reported a recoverable energy density as high as 17.4 J/cm^3 in the α-Fe_2O_3 nanoparticles doped $PbZrO_3$ thin film at 600 kV/cm.[10] Ge *et al.* found that the energy storage density and the energy efficiency of $Pb_{0.97}La_{0.02}(Zr_{0.95}Ti_{0.05})O_3$ film can be, respectively, enhanced to 14.8 J/cm^3 at 1 MV/cm and 66% by using oxide metal $LaNiO_3$ as top electrodes instead of Pt.[11]

On the other hand, the antiferroelectric-to-ferroelectric phase transition occurring in the antiferroelectric material is usually accompanied by a large volume change.[13] An external strain/stress can also effectively change the critical field of phase transition. Many researchers have investigated the influences of applied strain/stress on properties of the ferroelectric films.[14–18] However, only a few works have systematically studied this issue in antiferroelectric bulk or films.[19–21] Tan *et al.* found that the critical electric fields, i.e., E_{AF} for the antiferroelectric-to-ferroelectric phase transition and E_{FA} for the reverse transition, are shifted to high values by exerting the uniaxial or radial compressive stresses on the ceramic composition of $Pb_{0.99}Nb_{0.02}[(Zr_{0.57}Sn_{0.43})_{0.94}Ti_{0.06}]_{0.98}O_3$,[20] which leads to the increase of energy storage density in the antiferroelectric capacitor.[22] Ayyub *et al.* found that $PbZrO_3$ film presents ferroelectricity when its thickness is below 400 nm and show an-

*Project supported by the National Natural Science Foundation of China (Grant Nos. 11374312, 51401230, and 51522105) and the Fund for Ningbo Municipal Science and Technology Innovation Team, China (Grant No. 2015B11001).

†Corresponding author. E-mail: zhanqf@nimte.ac.cn

‡Corresponding author. E-mail: Runweili@nimte.ac.cn

© 2016 Chinese Physical Society and IOP Publishing Ltd

tiferroelectric behavior for the thickness above 550 nm due to the internal stresses caused by the substrate-clamping effect and their relaxation with thickness, which may result in the different energy storage densities and efficiencies for $PbZrO_3$ films at various thicknesses.[19] After removing the stress by the substrate clamping, the energy storage properties of freestanding film may be changed. So far, a lot of freestanding ferroelectric films have been prepared by different methods.[23–25] In this paper, we fabricated antiferroelectric $Pb(Zr_{0.95}Ti_{0.05})O_3$(PZT(95/5)) films on both Pt foils and platinized Si substrates by using pulsed laser deposition. In comparison with those of the substrate-clamped reference sample (C-PZT(95/5)), the E_{AF} and E_{FA} of freestanding film (F-PZT(95/5)) are remarkably enhanced while its saturation polarization is slightly reduced. As a result, the energy storage density and the energy storage efficiency of the F-PZT(95/5) film are both significantly enhanced.

2. Experimental procedure

In our experiment, 200-nm-thick Pt foils, which were used as both the flexible substrates and the bottom electrodes, were obtained by etching platinized Si wafers (Pt(200 nm)/Ti(50 nm)/SiO_2(500 nm)/Si) in 10 wt% HF solutions for 4 h. Due to the dissolution of the Ti layer and SiO_2 layer in HF solutions, the thin Pt foils were detached from the wafers. The Pt foil was then transferred to a thermal oxide silicon wafer. The detailed procedures for preparing Pt foils were described in our previous publication.[17] The 300-nm-thick antiferroelectric $Pb(Zr_{0.95}Ti_{0.05})O_3$ films were grown on the Pt foils by pulsed laser deposition at 560 °C and 10-Pa oxygen pressure, with a KrF excimer laser (248 nm, Coherent Inc.) running at a repetition rate of 5 Hz and an energy density of 2.3 J/cm^2. In order to characterize the electrical behaviors of antiferroelectric film, an array of circular Cu top electrodes (100 nm in thickness and 100 μm in diameter) was deposited on a PZT(95/5) layer with a metal shadow mask by e-beam evaporation. For comparison, 300-nm-thick C-PZT(95/5) film grown on platinized Si substrate was also prepared using the same parameters. The crystalline structures were characterized by an x-ray diffractometer (D8 Advance, Bruker) with Cu K_α radiation. The ferroelectric properties of F-PZT(95/5) and C-PZT(95/5) films were measured by a standardized ferroelectric test system (Precision Premier II, Radiant Technologies). Direct current (DC) electric field dependence of dielectric properties of the antiferroelectric films were measured by using a Keithley 4200 parameter analyzer.

3. Results and discussion

Figure 1(a) shows the XRD patterns of both F-PZT(95/5) and C-PZT(95/5) films. The XRD results illustrate that both samples possess the pure polycrystalline tetragonal PZT(95/5) phase. The splitting diffraction peaks of PZT(95/5)(001)/(100) and PZT(95/5) (002)/(200) appear around 22° and 44° for both films, respectively, as shown in Figs. 1(b) and 1(c). Similar observations have also been reported in $PbZrO_3$ bulk ceramic and $Pb_{0.99}Nb_{0.02}(Zr_{0.85}Sn_{0.13}Ti_{0.02})_{0.98}O_3$ films, which is ascribed to the tetragonal distortion of the orthorhombic lattice of antiferroelectrics.[26–28] The intensities of (100) and (200) diffraction peaks for F-PZT(95/5) films are much higher than those of (001) and (002) diffraction peaks, but for the C-PZT(95/5) films the intensities of (100) and (200) peaks are lower than those of (001) and (002) peaks. The variations in the intensity of diffraction peaks suggest that the C-PZT(95/5) films are *c*-axis-preferred oriented, but after removing the rigid substrates the F-PZT(95/5) films change to the preferred orientation of *a* axis. As displayed in the inset of Fig. 1(a), the (111) diffraction peak of F-PZT(95/5) film shifts about 0.12° toward the high angle in comparison with that of C-PZT(95/5) film, which suggests that the C-PZT(95/5) film suffers an out-of-plane tensile strain of 0.27% and an in-plane compressive strain of −0.13%. However, the strain caused by the substrate clamping effect is relaxed in the F-PZT(95/5) film.

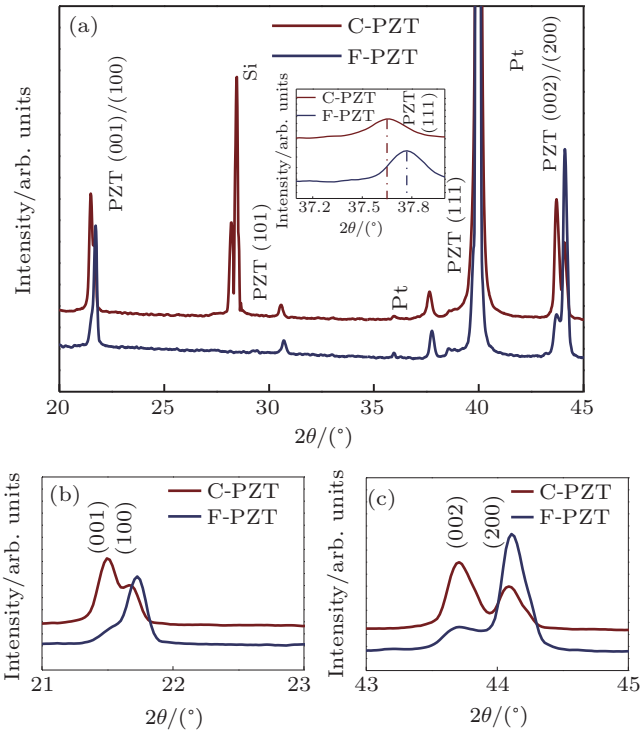


Fig. 1. (color online) (a) X-ray diffraction patterns of both free-standing F-PZT(95/5) film and substrate-clamped C-PZT(95/5) film. The inset shows a magnified view of PZT(95/5) (111) peak. The magnified views of (b) PZT(95/5) (001) and (100) peaks, and (c) PZT(95/5) (002) and (200) peaks.

Such a change in structure of PZT(95/5) thin film should have a significant influence on its electrical properties. To bridge the structural and electrical properties in the antiferroelectric materials, polarization hysteresis loops of F-PZT(95/5) and C-PZT(95/5) films are measured at 10 kHz

and at room temperature as shown in Fig. 2. Both samples exhibit the distinct features of double P–E hysteresis loops and small remanent polarizations (2.7 μC/cm^2 for F-PZT(95/5) and 1.7 μC/cm^2 for C-PZT(95/5)), which indicates that both films are antiferroelectric at room temperature. For the C-PZT(95/5) film, the antiferroelectric-to-ferroelectric phase transition occurs at $E_{AF} = 360$ kV/cm and the ferroelectric-to-antiferroelectric phase transition appears at $E_{FA} = 160$ kV/cm, which are determined by the peak value of the differentiation of the P–E loop. After removing the substrates, the E_{AF} and E_{FA} for F-PZT(95/5) films change to 770 kV/cm and 410 kV/cm, respectively, which are significantly increased as compared with those of C-PZT(95/5) film. The saturation polarizations of both F-PZT(95/5) and C-PZT(95/5) films are 31.3 μC/cm^2 and 32.9 μC/cm^2, respectively. It should be noted that the breakdown electric field of C-PZT(95/5) film is much lower than that of F-PZT(95/5) film. Thus the different maximum electric fields are used for the electrical characterizations of C-PZT(95/5) and F-PZT(95/5) films. The changes in the E_{AF} and E_{FA} can be understood by taking into account the rotation of dipole moments under the external stress. For antiferroelectric C-PZT(95/5) film which suffers an in-plane compressive stress caused by the rigid substrate, the c axis, i.e., the ⟨001⟩ direction of PZT(95/5), is easy to align out of plane.[29] During the antiferroelectric-to-ferroelectric phase transition, the c axis of the PZT(95/5) unit cell expands while the a-axis shrinks.[30,31] Therefore, the relaxation of in-plane compressive stress/strain in F-PZT(95/5) films acts against the antiferroelectric-to-ferroelectric phase transition. As a result, after removing the substrates, the E_{AF} and E_{FA} of F-PZT(95/5) films become larger than those of C-PZT(95/5) films.

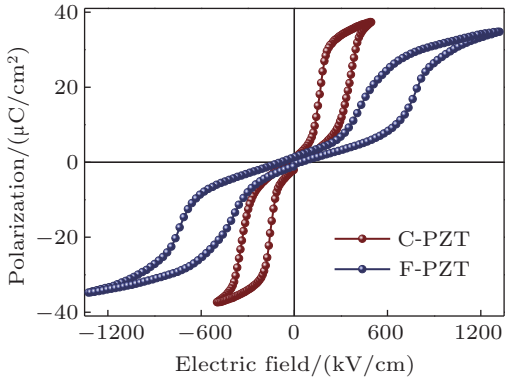


Fig. 2. (color online) Polarization hysteresis loops of antiferromagnetic F-PZT(95/5) and C-PZT(95/5) film.

As is well known, the electric displacement reflects the dipole orientation, while the dielectric constant indicates the motion of these dipoles. For a linear dielectric material, the dielectric constant can be related to the electric polarization as follows:

$$\varepsilon_r = \frac{1}{\varepsilon_0}\frac{\partial P}{\partial E},$$

where ε_r is the relative dielectric constant, ε_0 is the vacuum dielectric constant, P is the polarization, and E is the applied electric field. This relationship is generally invalid for nonlinear ferroelectric and antiferroelectric materials because the electric polarization changes irreversibly with electric field. However, in previous studies, $(\partial P/\partial E)/\varepsilon_0$ has been used to qualitatively account for ε_r at various electric fields in PVDF and PVDF-TrFE.[32,33] We herein use $(\partial P/\partial E)/\varepsilon_0$ to qualitatively evaluate the dielectric constant of antiferroelectric PZT(95/5) film. The corresponding results of $(\partial P/\partial E)/\varepsilon_0$ each as a function of the electric field for both F-PZT(95/5) and C-PZT(95/5) films are shown in Figs. 3(a) and 3(b), respectively. The peaks of $(\partial P/\partial E)/\varepsilon_0$ are located at the critical electric fields where the antiferroelectric-to-ferroelectric and ferroelectric-to-antiferroelectric phase transitions occur. In experiment, the electric field dependent dielectric constant of antiferroelectric PZT(95/5) film is obtained by the capacitance versus electric field (C–E) characterization through using the relation $\varepsilon_r = Ct/\varepsilon_0 A$, where C is the capacitance, t is the thickness of dielectric film, ε_0 is the vacuum permittivity, and A is the area of the capacitor as shown in Figs. 3(c) and 3(d). The peaks in ε_r–E curves of C-PZT(95/5) and F-PZT(95/5) films indicate the phase transition between the antiferroelectric and ferroelectric phases. Accordingly, the E_{AF} and E_{FA} based on the C–E measurement for C-PZT(95/5) film are 380 kV/cm and 150 kV/cm, respectively. For F-PZT(95/5) film, the E_{AF} and E_{FA} of F-PZT(95/5) film are changed to 550 kV/cm and 210 kV/cm, respectively. Both C–E and P–E measurements consistently show that the E_{AF} and E_{FA} of antiferroelectric PZT(95/5) film are increased after removing the strong clamping of substrate. The different values of critical fields determined from the two methods may result from the two different measurement mechanisms. The P–E curves are measured with a triangle wave while the C–E curves are measured with a DC bias plus a weak alternating current (AC) wave of 30 mV.[34,35]

The energy storage density W of an antiferroelectric material can be obtained from the hysteresis P–E loop by using the relation

$$W = \int_{P_r}^{P_{max}} E\,\mathrm{d}P,$$

where P_{max} and P_r are the polarization P measured at the highest electric field E_{max} and $E = 0$, respectively.[36] The energy loss density is determined by the area enclosed by the P–E loop, and the total energy density is the sum of the energy storage density and the energy loss density. The energy efficiency is defined as the ratio of the energy storage density to the total energy density. Figure 4(a) shows the variations of P_{max} with E_{max} for F-PZT(95/5) and C-PZT(95/5) film. With increasing the applied field, P_{max} exhibits three distinct increase rates in different regions of electric field, which corresponds to the an-

tiferroelectric states at low electric field, the antiferroelectric-to-ferroelectric phase transition around the E_{AF}, and the ferroelectric state at large electric field, respectively. The electric field dependences of the energy storage density W of F-PZT(95/5) and C-PZT(95/5) film are calculated from the P–E curves measured at different E_{max} (see Fig. 4(b)). The energy storage density W shows a similar increase rate as P_{max} in each range of applied field. The values of P_{max} and W of C-PZT(95/5) and F-PZT(95/5) thin films are small and increase slightly at low applied field since the applied electric field is too weak to induce the antiferroelectric-to-ferroelectric phase transition. With further increasing the electric field, P_{max} and W increase rapidly during the occurrence of antiferroelectric-to-ferroelectric phase transition. At high electric field, P_{max} and W increase slowly, for the polarization of PZT(95/5) film at ferroelectric state reaches saturation.

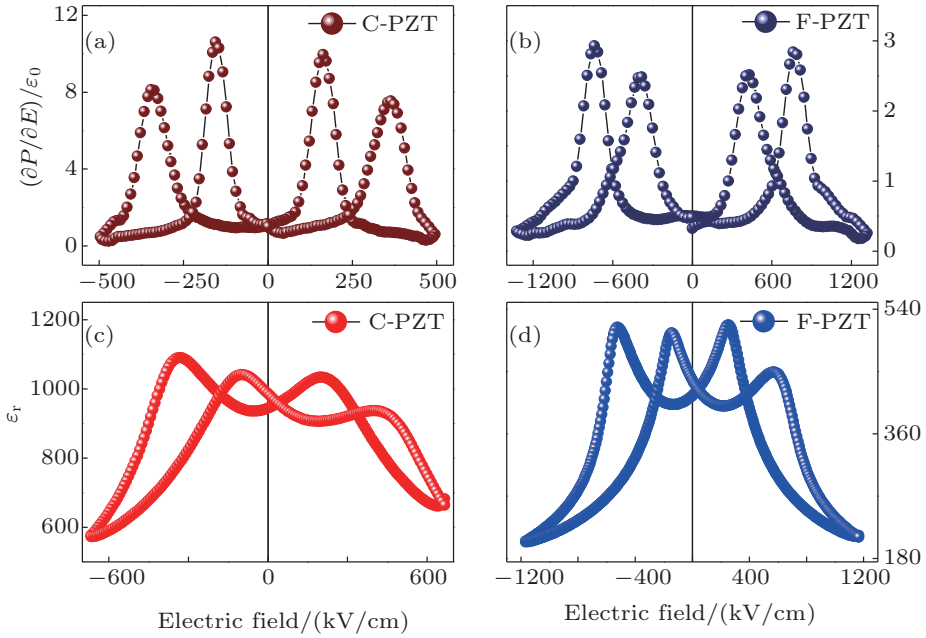


Fig. 3. (color online) Electric field dependences of $(\partial P/\partial E)/\varepsilon_0$ for (a) C-PZT(95/5) and (b) F-PZT(95/5) film, obtained by polarization hysteresis loops. Electric field dependences of dielectric constant for (c) C-PZT(95/5) and (d) F-PZT(95/5) film, obtained by the capacitance–electric field measurement.

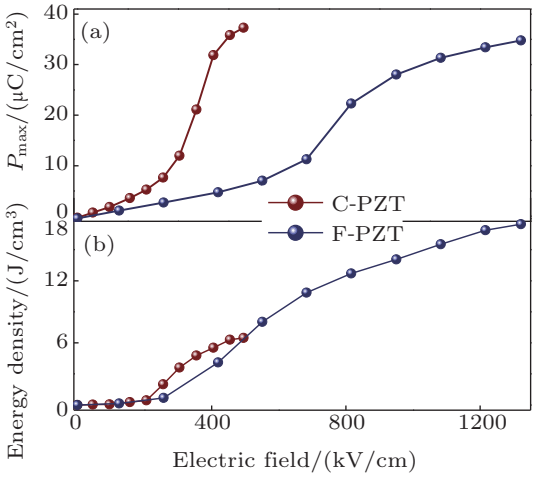


Fig. 4. (color online) Variations of (a) maximum polarization P_{max} and (b) the calculated energy storage density with electric field of F-PZT(95/5) and C-PZT(95/5) film, measured at different maximum electric fields.

Table 1. Energy storage properties of both C-PZT(95/5) and F-PZT(95/5) membranes.

Samples	Total energy density/(J/cm^3)	Energy storage density/(J/cm^3)	Energy loss density/(J/cm^3)	Energy Efficiency/%
C-PZT(95/5)	11.9	6.49	5.41	54.5
F-PZT(95/5)	25.67	17.45	8.22	67.9

As shown in Table 1, when a saturation electric field of 500 kV/cm is applied to the C-PZT(95/5) film, the total energy, energy storage and energy loss are 11.9 J/cm^3, 6.49 J/cm^3, and 5.41 J/cm^3, respectively. In contrast, when a saturation electric field of 1300 kV/cm is applied to the F-PZT(95/5) film, the total energy, energy storage and energy loss are 25.67 J/cm^3, 17.45 J/cm^3, and 8.22 J/cm^3, respectively. Compared with those of the C-PZT(95/5) film, the energy storage density and the energy loss density of F-PZT(95/5) film are enhanced by 10.96 J/cm^3 and 2.81 J/cm^3, respectively. Consequently, the energy efficiency of F-PZT(95/5) film reaches 67.9%. The enhanced energy storage properties of F-PZT(95/5) film after the relaxation of stress can be understood from the displacements of Zr^{4+} and Ti^{4+} atoms. In an ABO_3 perovskite structure, the ferroelectric polarization originates from the displacements of B^{4+} ions from the equilibrium B sites. For antiferroelectric PZT(95/5) film, Pb^{2+} ions occupy the A sites and Zr^{4+} and Ti^{4+} ions occupy the B sites. During antiferroelectric-to-ferroelectric transition, the lattice parameter a decreases while c increases. The XRD patterns show that C-PZT(95/5) film is c-axis-preferred oriented, but the F-PZT(95/5) films change to the preferred orientation of a axis. An in-plane

compressive strain exists in the C-PZT(95/5) film, which benefits the antiferroelectric-to-ferroelectric transition. After relaxation of the in-plane compressive stress in F-PZT(95/5) film, the coulomb interaction between two O^{2-} ions at the opposite vertices of octahedral becomes stronger, which causes the Pb^{2+} ions at A site to be hard to displace from the *ab* plane to ⟨111⟩ direction during the antiferroelectric-to-ferroelectric phase transition. As a result, compared with in C-PZT(95/5) film, a higher electric field is needed to induce the antiferroelectric-to-ferroelectric phase transition in F-PZT(95/5) film, which therefore increases both the energy storage density and the energy storage efficiency of the F-PZT(95/5) film after removing the substrate and relaxing the substrate clamping.

4. Conclusions

In this work, 300-nm-thick free-standing antiferroelectric PZT(95/5) film is successfully prepared on 200-nm-thick Pt foils by the pulsed laser deposition. The intensities of the (100) and (200) diffraction peaks of the F-PZT(95/5) film are increased after removing the substrate, indicating that F-PZT(95/5) film possesses an *a-axis*-preferred orientation. The antiferroelectric-to-ferroelectric electric field of the F-PZT(95/5) film increases up to 770 kV/cm compared with that of the substrate-clamped C-PZT(95/5) film. Therefore, the energy storage density and the energy storage efficiency are enhanced to 17.45 J/cm^3 and 67.9%, respectively. Using the wafer bonding technology, the free-standing C-PZT(95/5) films can be integrated on any kind of flexible substrates, making them available for applications in flexible electrical devices such as capacitors and actuators.

References

[1] Chen X F, Cao F, Zhang H L, Yu G, Wang G S, Dong X L, Gu Y, He H L and Liu Y S 2012 *J. Am. Ceram. Soc.* **95** 1163

[2] Yao K, Chen S T, Rahimabady M, Mirshekarloo M S, Yu S H, Tay F E H, Sritharan T and Lu L 2011 *IEEE Trans. Ultrason. Ferroelectr. Freq. Control.* **58** 1968

[3] Liu Y Y, Lu X M, Jin Y M, Peng S, Huang F Z, Kan Y, Xu T T, Min K L and Zhu J S 2012 *Appl. Phys. Lett.* **100** 212902

[4] Shirane G, Sawaguchi S and Takagi Y 1951 *Phys. Rev.* **84** 476

[5] Jaffe B 1961 *Proc. IRE* **49** 1264

[6] Xu B, Moses P, Pai N G and Cross L E 1998 *Appl. Phys. Lett.* **72** 593

[7] Sternberg A, Kundzinsa K, Zaulsa V and Aulikaa I 2004 *J. Eur. Ceram. Soc.* **24** 1653

[8] Parui J and Krupanidhi S B 2008 *Appl. Phys. Lett.* **92** 192901

[9] Jiang S J, Zhang L, Zhang G Z, Liu S S, Yi J Q, Xiong X, Yu Y, He J G and Zeng Y K 2013 *Ceram. Int.* **39** 5571

[10] Sa T L, Cao Z P, Wang YJ and Zhu H B 2014 *Appl. Phys. Lett.* **105** 043902

[11] Ge J, Dong X L, Chen Y, Cao F and Wang G S 2013 *Appl. Phys. Lett.* **102** 142905

[12] Ge J, Pan G, Remiens D, Chen Y, Cao F, Dong X L and Wang G S 2012 *Appl. Phys. Lett.* **101** 112905

[13] Pan W Y, Dan C Q, Zhang Q M and Cross L E 1989 *J. Appl. Phys.* **66** 6014

[14] Jang H W, Baek S H, Ortiz D, Folkman C M, Eom C B, Chu Y H, Shafer P, Ramesh R, Vaithyanathan V and Schlom D G 2008 *Appl. Phys. Lett.* **92** 062910

[15] Ryu J, Priya S, Park C S, Kim K Y, Choi J J, Hahn B D, Yoon W H, Lee B K, Park D S and Park C 2009 *J. Appl. Phys.* **106** 024108

[16] Lee J W, Park C S, Jo J H and Kim H E 2007 *Appl. Phys. Lett.* **91** 072903

[17] Zuo Z H, Chen B, Zhan Q F, Liu Y W, Yang H L, Li Z X, Xu G J and Li R W 2012 *J. Phys. D: Appl. Phys.* **45** 185302

[18] Griggio F, Jesse S, Kumar A, Ovchinnikov O, Kim H, Jackson T N, Damjanovic D, Kalinin S V and Trolier-McKinstry S 2012 *Phys. Rev. Lett.* **108** 157604

[19] Ayyub P, Chattopadhyay S, Pinto R and Multani M S 1998 *Phys. Rev. B* **57** R5559

[20] Tan X, Frederick J, Ma C, Aulbach E, Marsilius M, Hong W, Granzow T, Jo W and Rödel J 2010 *Phys. Rev. B* **81** 014103

[21] Ge J, Remiens D, Dong X L, Chen Y, Costecalde J, Gao F, Cao F and Wang G S 2014 *Appl. Phys. Lett.* **105** 112908

[22] Kwon S, Hackenberger W, Alberta E, Furman E and Lanagan M 2011 *IEEE Electr. Insul. Mag.* **27** 43

[23] Jang H W, Baek S H, Ortiz D, Folkman C M, Eom C B, Chu Y H, Shafer P, Ramesh R, Vaithyanathan V and Schlom D G 2008 *Appl. Phys. Lett.* **92** 062910

[24] Ryu J, Priya S, Park C S, Kim K Y, Choi J J, Hahn B D, Yoon W H, Lee B K, Park D S and Park C 2009 *J. Appl. Phys.* **106** 024108

[25] Lee J W, Park C S, Jo J H and Kim H E 2007 *Appl. Phys. Lett.* **91** 072903

[26] Hao X H, Zhai J W, Zhou F, Song X W and An S L 2010 *J. Sol-Gel Sci. Technol.* **53** 366

[27] Fujishita H, Shiozaki Y and Sawaguchi E 1979 *J. Phys. Soc. Jpn.* **46** 1391

[28] Xu B, Cross L E and Ravichandran D 1999 *J. Am. Ceram. Soc.* **82** 306

[29] Hall D A, Evans J D S, Oliver E C, Withers P J and Mori T 2007 *Philos. Mag. Lett.* **87** 41

[30] Blue C T, Hicks J C, Park S E, Yoshikawa S and Cross L E 1996 *Appl. Phys. Lett.* **68** 2942

[31] Park S E, Pan M J, Markowski K, Yoshikawa S and Cross L E 1997 *J. Appl. Phys.* **82** 1798

[32] Guan F X, Pan J L, Wang J, Wang Q and Zhu L 2010 *Macromolecules* **43** 384

[33] Furukawa T, Lovinger A J, Davis G T and Broadhurst M G 1983 *Macromolecules* **16** 1885

[34] Hao X H, Zhai J W, Chou X J and Yao X 2007 *Solid State Commun.* **142** 498

[35] Li X, Zhai J W and Chen H 2005 *J. Appl. Phys.* **97** 024102

[36] Burn I and Smyth D M 1972 *J. Mater. Sci.* **7** 339